

# IPDreamer: Appearance-Controllable 3D Object Generation with Image Prompts

Bohan Zeng<sup>1†</sup>, Shanglin Li<sup>1†</sup>, Yutang Feng<sup>1†</sup>, Hong Li<sup>1</sup>, Sicheng Gao<sup>1</sup>, Jiaming Liu<sup>3</sup>, Huaxia Li<sup>3</sup>, Xu Tang<sup>3</sup>, Jianzhuang Liu<sup>4</sup>, Baochang Zhang<sup>1,2,5\*</sup>

<sup>1</sup> Beihang University, Beijing, China

<sup>2</sup> Nanchang Institute of Technology, Nanchang, China

<sup>3</sup> Xiaohongshu Inc

<sup>4</sup> Shenzhen Institute of Advanced Technology, Shenzhen, China

<sup>5</sup> Zhongguancun Laboratory, Beijing, China

{bohanzeng, shanglin, yutangfeng, bczhang}@buaa.edu.cn

**Abstract.** Recent advances in 3D generation have been remarkable, with methods such as DreamFusion leveraging large-scale text-to-image diffusion-based models to supervise 3D generation. These methods enable the synthesis of detailed and photorealistic textured objects. However, the appearance of 3D objects produced by these text-to-3D methods is unpredictable, and it is hard for the single-image-to-3D methods to deal with complex images, thus posing a challenge in generating appearance-controllable 3D objects. To achieve controllable complex 3D object synthesis, we introduce IPDreamer, a novel approach that incorporates **Image Prompts** to provide specific and comprehensive appearance information for 3D object generation. Our results demonstrate that IPDreamer effectively generates high-quality 3D objects that are consistent with both the provided text and the appearance of complex image prompts, demonstrating its promising capability in appearance-controllable 3D object generation. Our code is available at <https://github.com/zengbohan0217/IPDreamer>.

**Keywords:** 3D objects synthesis · Image prompts adaption

## 1 Introduction

The rapid evolution of 3D technology has revolutionized the way we create and interact with virtual worlds. 3D technology is now essential in a wide range of fields, including architecture, gaming, mechanical manufacturing, and AR/VR. However, creating high-quality 3D content remains a challenging and time-consuming task, even for experts. To address this challenge, researchers have developed text-to-3D methodologies that automate the process of generating 3D assets from textual descriptions. Built on the 3D scene representation capabilities of Neural Radiance Fields (NeRFs) [33, 37] and the rich visual prior knowledge of pretrained diffusion models [48, 49], recent research [6, 20, 25, 34, 43, 64]

† Equal contribution.

\* Corresponding author.

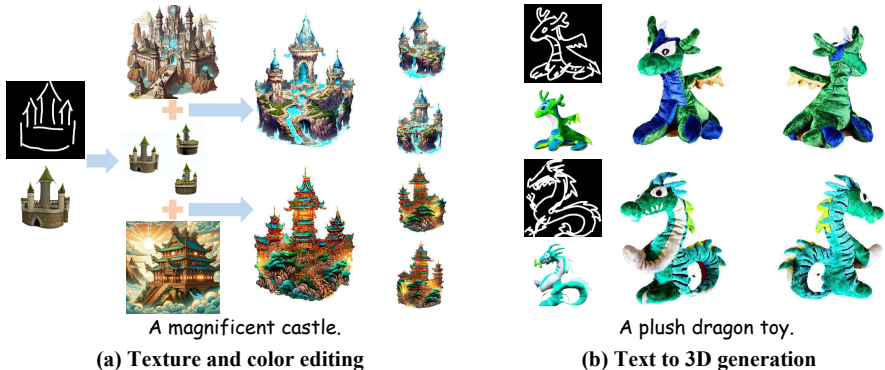


**Fig. 1:** IPDREAMER can generate controllable, desired, and high-quality 3D objects based on given textual and image prompts. (a) Two high-quality 3D objects with rich details, which are initialized by the same NeRF model and guided by the complex reference image prompts (second column). (b) Two text-to-3D examples with the same text prompt. IPDREAMER generates two different 3D objects following the guidance of the two different image prompts (first column), respectively.

has made significant progress, simplifying the text-to-3D pipeline and making it more accessible, which causes a significant shift in these fields.

Recent advances in diffusion models have significantly enhanced the capabilities of text-to-image generation. State-of-the-art (SOTA) systems, leveraging cutting-edge diffusion-based techniques [1, 18, 40, 48, 69], can now generate and modify images directly from textual descriptions with vastly improved quality and controllability. Inspired by the rapid development of text-to-image generation, recent works [6, 25, 43] utilize pretrained text-to-image diffusion models and the Score Distillation Sampling (SDS) algorithm to optimize 3D representations. The rendering results of these optimized representations are more photorealistic than those optimized by CLIP models [20, 34].

To address the over-smoothing and low-diversity problems of SDS, ProlificDreamer [64] proposes Variational Score Distillation (VSD) for high-quality and more diverse 3D scene and object synthesis. VSD learns a parametric score model and treats the given textual prompt as a random variable instead of a single point as in SDS. By adding variables corresponding to the camera information for rendering images, VSD effectively addresses the over-smoothing issue in SDS. Although ProlificDreamer can generate impressive 3D objects from text conditions, the appearance of its generated results is uncontrollable due to the randomness in the training process of the Low-Rank Adaptation (LoRA) model [18] adopted in VSD.

Unlike the unpredictability in text-to-3D generation, single-image-to-3D generation allows for strict control over the appearance of the generated 3D results. However, existing single-image-to-3D methods [28, 29, 52] are limited to handling simple images containing clearly defined objects, often struggling with complex

images. For example, they cannot deal with the complex images provided in Fig. 1(a).

To solve these problems, we propose *IPDreamer*, a novel approach that incorporates image prompts to provide specific and comprehensive appearance<sup>1</sup> information for 3D generation. This approach enables controllable production of high-quality 3D objects, guided by complex images.

Recently, some methods [62, 67, 70] use image prompts to modify the cross attention in diffusion models for better control of image generation. In this paper, we extend SDS to *Image Prompt Score Distillation* (IPSD), which leverages image prompts to guide the optimization of 3D object appearance. With the proposed IPSD, IPDreamer can utilize any complex image to obtain appearance-controllable and high-quality 3D object generation.

Specifically, our IPDreamer initiates the process by generating 2D guidance images, the characteristics of which can be selected or controlled by the user. Next, we create a coarse NeRF model [33] by leveraging the multiview generation capability of Zero-1-to-3 [28] which can provide a 3D prior for the NeRF model. Finally, we utilize IP-Adapter to extract image prompt embeddings from the 2D images and their corresponding normal maps. These prompts guide the optimization of the texture and geometry of the 3D meshes, respectively.

As illustrated in Fig. 1(a), IPDreamer is capable of transferring the styles of complex reference images to the NeRF model and generating high-quality 3D objects. In Fig. 1(b), IPDreamer generates two 3D objects corresponding to the image prompts (first column) under the same textual prompt. These two parts demonstrate the efficacy of using image prompts for guiding texture optimization.

In summary, the main contributions of this paper are as follows:

- We present a novel 3D object synthesis framework, IPDreamer, that empowers users to synthesize controllable and high-quality 3D objects more easily.
- We introduce Image Prompt Score Distillation (IPSD), which utilizes image prompt adaption to guide 3D mesh generation and provides substantial appearance information.
- Our IPDreamer has the capability of generating a high-quality 3D object whose style is aligned with a provided image prompt, which cannot be achieved in previous methods.
- Comprehensive experiments demonstrate that IPDreamer achieves high-quality 3D generation and impressive rendering results, outperforming existing SOTA methods.

---

<sup>1</sup> In this paper, the appearance of an object/scene includes its shape, texture, and color.

## 2 Related Works

### 2.1 Diffusion Models

Diffusion models (DMs) are initially introduced as a generative model that gradually denoises images corrupted by Gaussian noise to produce samples [53]. Recent advances in DMs [8, 16, 42, 48, 54, 61] have demonstrated their superior performance in image synthesis. DMs have also achieved SOTA in other synthesis tasks, such as text-to-image generation [40], inpainting [30, 67], 3D object synthesis [24, 31], video synthesis [15, 17], speech synthesis [21, 26], super-resolution [10, 23, 50], face animation [44], text-to-motion generation [58], and brain signal visualization [55, 56]. There are also DMs [22, 63] that generate diverse results by learning the internal patch distribution from a single image. Null-text-inversion [35] improves image editing with diffusion pivotal inversion and null-text optimization. These advances demonstrate the versatility and potential of DMs for a wide range of synthesis tasks.

### 2.2 Controllable Generation and Editing

Controllable generation and editing of 2D images and 3D objects is a core goal of generative tasks. With the emergence of large language models (LLMs) such as GPT-3 and Llama [2, 59, 60], instruction-based user-friendly generative control has gained much attention. InstructPix2Pix [1] and MagicBrush [68] build datasets based on LLMs and large text-to-image models to achieve effective instruction control on 2D images. InstructNeRF2NeRF [13] combines this method with NeRF scene reconstruction [33] to introduce instruction control into 3D generation.

Meanwhile, a series of adapter methods such as ControlNet and IP-Adapter [18, 19, 36, 67, 69, 72] provide reliable approaches for fine-tuning large pre-trained DMs (e.g., Stable Diffusion [48] and Imagen [49]) for conditional controllable generation (e.g., using sketch, canny, pose, etc. to control image structure). Among them, IP-Adapter [67] introduces a decoupled cross-attention mechanism to achieve effective appearance generation control using image prompts. In this paper, we use IP-Adapter to provide effective appearance control for generating 3D objects from given images and text prompts.

### 2.3 3D Generation

In recent years, 3D generative modeling has attracted a large number of researchers. Inspired by the recent neural volume rendering, many 3D-aware image rendering methods [3, 4, 11, 12, 39, 41] are proposed to generate high-quality rendered 2D images for 3D visualization. Meanwhile, with the development of text-to-image synthesis, researchers have shown a growing interest in text-to-3D generation. Early methods such as DreamField [20] and CLIPmesh [34] achieve text-to-3D generation by utilizing a pretrained image-text aligned model CLIP [46].



They optimize the underlying 3D representations (NeRFs and meshes) to ensure that all 2D renderings have high text-image alignment scores.

Recently, [5, 6, 25, 43, 64] have achieved high-quality 3D synthesis (NeRFs and meshes) by leveraging a robust pretrained text-to-image DM as a strong prior to guide the training of the 3D model. Other works [28, 52, 71] introduce multi-view DMs to enhance 3D consistency and provide strong structured semantic priors for 3D synthesis. IT3D [7] combines SDS and GAN to refine the 3D model and obtain high-quality 3D synthesis. Additionally, [27, 32, 45, 57] are capable to generate 3D representations based on single images, and [28, 29, 52, 66] achieve 2D images in multiple viewpoints, which enable consistent 3D object generation.

In this work, we find that the sufficient appearance information provided by image prompt features can effectively guide the synthesis of high-quality 3D objects. Therefore, we propose IPDreamer, which leverages image prompts to provide sufficient appearance information, enabling the synthesis of high-quality 3D objects.

### 3 Method

In this section, we present the details of IPDreamer. First, we give the problem statement of text-to-3D/single-image-to-3D generation and the preliminaries of SDS and VSD. Then, we briefly overview IPDreamer. Finally, we explain the training framework of our two-stage 3D generation, i.e., NeRF training and mesh training.

#### 3.1 Preliminaries

Given a text prompt  $y$  or an image  $I$ , text-to-3D/single-image-to-3D generation aims at synthesizing novel views and optimizing the parameters of a 3D object/scene that corresponds to the given  $y$  or  $I$ . DreamFusion [43] utilizes a pretrained text-to-image DM  $\epsilon_{pretrain}$  to optimize an MLP parameterized as  $\theta$  representing a 3D volume, where a differentiable generator  $g$  renders  $\theta$  to create 2D images  $x = g(\theta, c)$  given a sampled camera pose  $c$ , based on the gradient of the Score Distillation Sampling (SDS) loss:

$$\nabla_{\theta} \mathcal{L}_{\text{SDS}}(\theta) = \mathbb{E}_{t, \epsilon} \left[ w(t) (\epsilon_{pretrain}(x_t; y, t) - \epsilon) \frac{\partial x}{\partial \theta} \right], \quad (1)$$

where  $w(t)$  is a weighting function,  $\epsilon_{pretrain}(x_t; y, t)$  predicts the noise  $\epsilon \sim \mathcal{N}(0, I)$  given the noisy image  $x_t$ , text-prompt features  $y$  and timestep  $t$ . However, empirical observations [43] show that SDS often suffers from over-saturation, over-smoothing, and low-diversity problems. To address them, ProlificDreamer [64] proposes Variational Score Distillation (VSD), which treats the associated 3D scene as a random variable rather than a single point based on a textual prompt. Specifically, ProlificDreamer introduces a prediction network, denoted

as  $\epsilon_\phi$ , which is a trainable LoRA model [18] applied to the pretrained model  $\epsilon_{pretrain}$ . The optimization of  $\epsilon_\phi$  can be represented as:

$$\min \mathbb{E}_{t,\epsilon,c} [ \|\epsilon_\phi(x_t; y, t, c) - \epsilon\|_2^2 ], \quad (2)$$

and VSD computes the gradient of the VSD loss as:

$$\nabla_\theta \mathcal{L}_{\text{VSD}}(\theta) = \mathbb{E}_{t,\epsilon,c} [ w(t) (\epsilon_{pretrain}(x_t; y, t) - \epsilon_\phi(x_t; y, t, c)) \frac{\partial x}{\partial \theta} ]. \quad (3)$$

Although ProlificDreamer shows excellent ability of text-to-3D generation, the appearance of its 3D synthesis results is uncontrollable. A feasible solution to realize controllable 3D object generation is to use a 2D image as a prior. However, existing single-image-to-3D methods are difficult to obtain high-quality 3D object synthesis from complex single images. To address these problems, we employ the image prompt adaption method [67] to provide sufficient appearance information for 3D object synthesis. Specifically, we first obtain a coarse NeRF model, which can be generated with a pretrained DM (e.g., Stable Diffusion or Zero-1-to-3) with a textural prompt  $y$  or an image  $I_{rgb}$ . Then we extract the image prompt feature  $y_{rgb}$  from  $I_{rgb}$ . Based on  $y_{rgb}$ , IPDreamer can generate a highly detailed controllable 3D object with less training consumption compared to ProlificDreamer.

### 3.2 Overview of IPDreamer

We outline the proposed 3D object generation framework in Fig. 2(a), which has two main stages: NeRF training (Stage 1), and mesh training (Stage 2). The two-stage training aims to generate controllable 3D objects in a coarse-to-fine manner. In Stage 1 (Fig. 2(b)), we employ a NeRF to represent the shape and color of a 3D object. We leverage the multi-view knowledge within the Zero-1-to-3 model  $\epsilon_{zero123}$  [28] to train a coarse NeRF model that aligns with  $I_{rgb}$  which can be either provided by the user or generated by a text-to-image model with a textual prompt  $y$ . In Stage 2, we begin with extracting the 3D mesh from the NeRF using DM Tet [51]. By leveraging the appearance guidance capability of our proposed IPSD for 3D objects, we can replace  $I_{rgb}$  used in Stage 1 with another complex image to guide the synthesis of the 3D object. To optimize the geometry of the 3D mesh, we first obtain the normal image  $I_n$  from  $I_{rgb}$  by DPT [47]. Then we extract another image prompt feature  $y_n$  from  $I_n$  using the image encoder  $\mathcal{E}_{image}$  of IP-Adapter  $\epsilon_{ip}$ <sup>2</sup> [67]. This  $y_n$  is then used by  $\epsilon_{ip}$  to supervise the generation of the normal image  $x_{n,ran}$ . To optimize the texture of the 3D mesh, we utilize the image prompt features  $y_{rgb}$  and introduce a geometry prompt difference  $\delta_{geo}$  to supervise the rendering results  $x_{rgb}$  of the 3D mesh.

<sup>2</sup> We use  $\epsilon_{ip}$  to denote the denosing model of IP-Adapter to leverage the image prompt features.

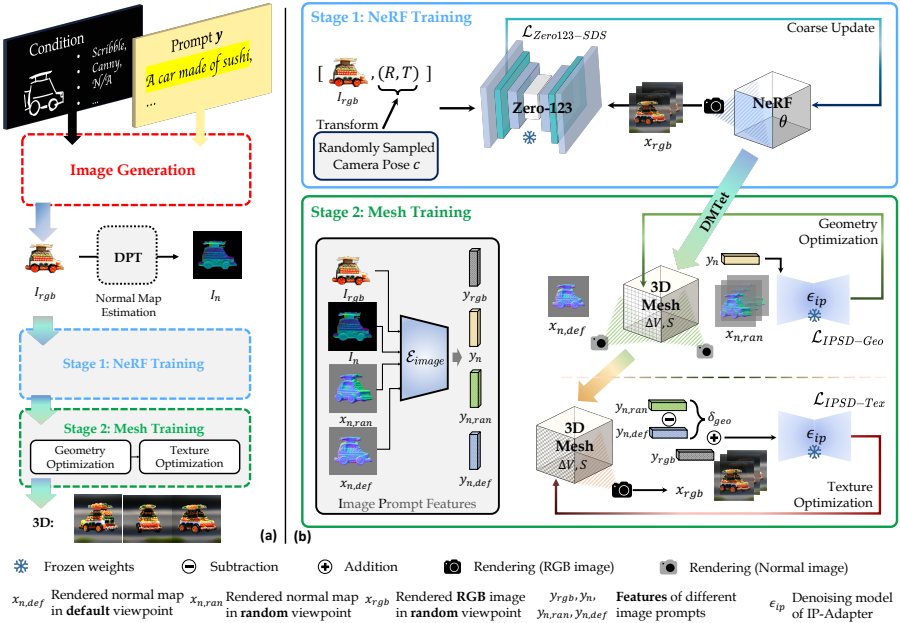


**Fig. 2: Overview of IPDreamer.** IPDreamer is designed to generate high-quality, controllable 3D objects using a two-stage, coarse-to-fine approach. (a) *IPDreamer pipeline.* We first utilize Stable Diffusion and ControlNet [69] to generate an RGB image  $I_{rgb}$  based on the user-provided textual prompt and condition. Then we obtain the final 3D object through a two-stage training in a coarse-to-fine manner. (b) *Details of the two-stage training.* In Stage 1, we harness the multi-view knowledge integrated into the Zero-1-to-3 model to optimize the NeRF representation, ultimately yielding the coarse 3D model. In Stage 2, we extract the 3D mesh from the NeRF using DMTet [51], and then use IPSD to further optimize the geometry and texture of the high-resolution 3D mesh to achieve a desired 3D object.

### 3.3 NeRF Training

Before we optimize the 3D objects by *IPSD*, we need to obtain a NeRF model which can be either given or generated by a textual prompt  $y$  or an image  $I_{rgb}$ . To obtain a morphologically plausible 3D representation of the object, we employ Zero-1-to-3 to train this coarse NeRF model based on the image  $I_{rgb}$  generated by the given text prompt  $y$ . It is worth noting that obtaining a coarse NeRF model is not the main focus of this work. Leveraging the powerful guidance of *IPSD* for 3D mesh optimization, simply providing a basic coarse NeRF model is enough. Therefore, besides using Zero-1-2-3 for supervision, alternative methods can also be employed to acquire a coarse NeRF model.

*Image Generation.* With the current advancements in text-to-image generation and editing techniques, we now have a variety of methods available to create desired images that can be used to guide the 3D generation process. In this study, we utilize Stable Diffusion and ControlNet [69] to generate images based

on textual prompts and user-provided conditions. This approach allows users to have better control of the appearance of the 3D object according to the generated image prompt  $I_{rgb}$ .

*Training of the Coarse NeRF Model.* To ensure the consistency of the 3D object in different viewpoints, we adopt Zero-1-to-3, which can generate multi-view images based on a single image and corresponding rotation angles. Let  $x_{rgb}$  be the rendered image from a randomly sampled viewpoint. As shown in the upper box in Fig. 2(b), we utilize the SDS loss in conjunction with the Zero-1-to-3 model  $\epsilon_{zero123}$  to optimize the NeRF parameters  $\theta$ , with the following gradient:

$$\nabla_{\theta} \mathcal{L}_{\text{Zero123-SDS}}(\theta) = \mathbb{E}_{t,\epsilon} [w(t) (\epsilon_{zero123}(z_{rgb,t}; (I_{rgb}, R, T), t) - \epsilon) \frac{\partial z_{rgb}}{\partial \theta}], \quad (4)$$

where  $z_{rgb,t}$  denotes the noisy latent code of  $x_{rgb}$  in timestep  $t$  (we employ the encoder of Stable Diffusion [48] to encode the observed image into the latent code),  $R \in \mathbb{R}^{3 \times 3}$  and  $T \in \mathbb{R}^3$  respectively denote the relative camera rotation and translation from the default viewpoint (i.e., the viewpoint corresponding to  $I_{rgb}$ ) to a random viewpoint. Upon completing this training stage, we obtain a coarse yet view-consistent NeRF model.

### 3.4 Mesh Training

In this section, we disentangle the modeling and optimization of the geometry and texture of a 3D object. Formally, we represent the 3D shape using a deformable tetrahedral grid  $(V, T)$ , where  $V$  is the set of vertices and  $T$  is the set of tetrahedrons in the grid. Each vertex  $v_i \in V$  contains a signed distance field (SDF) value  $s_i \in S$  and a deformation  $\Delta v_i \in \Delta V$  of the vertex from its initial canonical coordinate. During optimization, we render the extracted surface mesh into a high-resolution image using the differentiable rasterizer [38]. We optimize  $\Delta V$ ,  $S$  and  $\theta$  via backpropagation using the IPSD gradients (Eq. 5, Eq. 6, Eq. 8, Eq. 9 and Eq. 10).

As shown in the lower box in Fig. 2(b), for geometry optimization, we render and encode the surface normal map extracted from DM Tet [51] as the input of  $\epsilon_{ip}$ , which can generate an object with more detail. For texture optimization, we utilize  $y_{rgb}$  and a geometry prompt difference  $\delta_{geo}$  to optimize the texture of the 3D object. Note that the  $I_{rgb}$  in this section can be replaced with any other complex image, as discussed in Fig. 4, which demonstrates the impressive guidance capability of *IPSD* for 3D object synthesis.

*Geometry Optimization.* Both Fantasia3D [6] and ProlificDreamer [64] optimize the estimated normal map using SDS for geometry optimization. However, optimizing the normal map with a text-to-image DM can be rather challenging because the DM’s pre-training dataset lacks normal map images. To address this, we adopt an additional normal image prompt feature  $y_n = \mathcal{E}_{image}(I_n)$  to provide richer and more reliable information for normal map optimization, instead of solely using the textual prompt  $y$  [6, 64].

The geometry optimization process computes the gradients of the IPSD geometry loss as:

$$\nabla_{\Delta V} \mathcal{L}_{\text{IPSD-Geo}}(\Delta V, S) = \mathbb{E}_{t,\epsilon}[w(t) (\epsilon_{ip}(z_{n,t}; y_n, y, t) - \epsilon) \frac{\partial z_n}{\partial \Delta V}], \quad (5)$$

$$\nabla_S \mathcal{L}_{\text{IPSD-Geo}}(\Delta V, S) = \mathbb{E}_{t,\epsilon}[w(t) (\epsilon_{ip}(z_{n,t}; y_n, y, t) - \epsilon) \frac{\partial z_n}{\partial S}], \quad (6)$$

where  $z_{n,t}$  denotes the noisy latent code of  $x_{n,ran}$  in timestep  $t$ . The IPSD (image prompt score distillation) geometry loss is an extension of the SDS loss [43], with  $\Delta V, S$  and  $y_n$  added. IPSD has a lower computational cost compared to VSD, as VSD requires the optimization of additional training parameters (i.e., the parameters of its LoRA model).

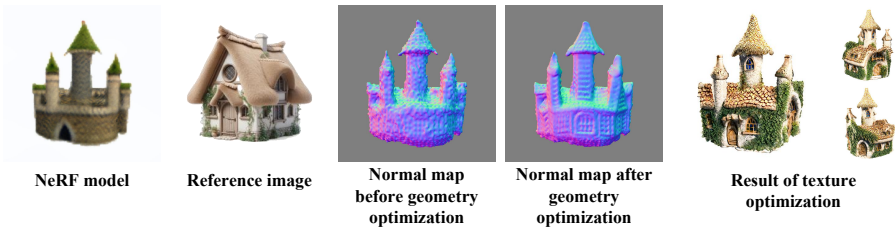


**Fig. 3:** An optimization example of IPDreamer.

*Texture Optimization.* After optimizing the estimated normal map, the shape of the 3D mesh becomes more reasonable. Then we further optimize the texture through IPSD. We first extract the image prompt features  $y_{rgb} = \mathcal{E}_{image}(I_{rgb})$ , as a basic guidance for the texture optimization. Then we devise a geometry prompt difference  $\delta_{geo}$  for  $y_{rgb}$  to compensate for the morphological disparity between  $x_{rgb}$  and  $I_{rgb}$ . Let  $x_{n,def}$ , and  $x_{n,ran}$  be the rendered normal map of the 3D mesh from the default viewpoint and a randomly sampled viewpoint, respectively. We extract their image prompt features,  $y_{n,def} = \mathcal{E}_{image}(x_{n,def})$  and  $y_{n,ran} = \mathcal{E}_{image}(x_{n,ran})$ . The difference between  $y_{n,ran}$  and  $y_{n,def}$  is called the geometry prompt difference  $\delta_{geo}$ :

$$\delta_{geo} = y_{n,ran} - y_{n,def}. \quad (7)$$

The texture optimization process computes the gradients of the IPSD texture loss as:

$$\begin{aligned} \nabla_{\theta} \mathcal{L}_{\text{IPSD-Tex}}(\theta, \Delta V, S) = \\ \mathbb{E}_{t,\epsilon}[w(t) (\epsilon_{ip}(z_{rgb,t}; y_{rgb} + \delta_{geo}, y, t) - \epsilon) \frac{\partial z_{rgb}}{\partial \theta}], \end{aligned} \quad (8)$$

$$\begin{aligned} \nabla_{\Delta V} \mathcal{L}_{\text{IPSD-Tex}}(\theta, \Delta V, S) = \\ \mathbb{E}_{t,\epsilon}[w(t) (\epsilon_{ip}(z_{rgb,t}; y_{rgb} + \delta_{geo}, y, t) - \epsilon) \frac{\partial z_{rgb}}{\partial \Delta V}], \end{aligned} \quad (9)$$

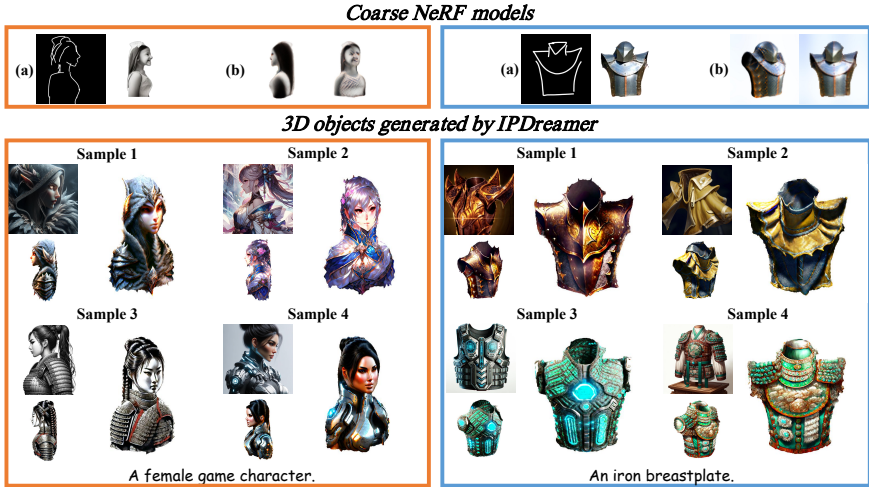


**Fig. 4:** Edited 3D objects with different image prompts. (a) Scribble object outlines and corresponding image prompts for NeRF models generation. (b) Rendering of NeRFs from Stage 1. We show four samples for each textual prompt. In each sample, the top left is a selected image prompt, and the bottom left and the right illustrate the 3D object optimized by IPDreameer based on the NeRF from Stage 1.

$$\begin{aligned} \nabla_S \mathcal{L}_{\text{IPSD-TeX}}(\theta, \Delta V, S) = \\ \mathbb{E}_{t, \epsilon} [w(t) (\epsilon_{ip}(z_{rgb,t}; y_{rgb} + \delta_{geo}, y, t) - \epsilon) \frac{\partial z_{rgb}}{\partial S}], \end{aligned} \quad (10)$$

where  $z_{rgb,t}$  denotes the noisy latent code of  $x_{rgb}$  (random viewpoint) in timestep  $t$ . The geometry prompt difference  $\delta_{geo}$  can effectively represent the Morphological distance between  $x_{n,ran}$  and  $x_{n,def}$  in the image prompt feature space. Thus it is used to compensate  $y_{rgb}$  (default viewpoint) such that  $y_{rgb} + \delta_{geo}$  represents the RGB image  $x_{rgb}$ .

To show the effectiveness of IPDreameer, we give a generation example of IPDreameer in Fig. 3, where we optimize the 3D object using a reference image prompt that has a different appearance from the NeRF model. It is evident that after geometry optimization, the originally rough geometric details of the NeRF model have been significantly improved. And after texture optimization, the coarse 3D object is transformed into a high-quality 3D object that matches the appearance of the reference image prompt.

## 4 Experiments

### 4.1 Texture Editing

In Stage 2 of our framework (see Fig. 2), after a NeRF is obtained in Stage 1, we can use another image prompt with a similar object but a different texture for



**Fig. 5:** More samples of 3D object editing. (a) Coarse NeRF models. (b) Provided image prompts. (c) 3D objects generated by IPDreamer.

**Table 1:** Quantitive comparison of text-to-3D generation.

Method	FID ↓	CLIP-Score ↑
DreamFusion	313.58	0.2532
Magic3D	328.00	0.2722
Fantasia3D	292.86	0.2690
ProlificDreamer	284.52	0.2725
IPDreamer(Ours)	<b>257.17</b>	<b>0.2859</b>

**Table 2:** Percentage of the preference in the user study.

Method	Prefer baseline	Prefer ours
DreamFusion	6.45	<b>93.55</b>
Magic3D	10.89	<b>89.11</b>
Fantasia3D	25.82	<b>72.18</b>
ProlificDreamer	41.65	<b>58.35</b>

texture editing. As depicted in Fig. 4, we show reconstructed 3D samples that use new image prompts to guide generation. This demonstrates IPDreamer’s ability to produce high-quality 3D objects that align with the styles of the provided images. Remarkably, IPDreamer can appropriately transfer the styles of the image prompts to the synthesized 3D objects, regardless of the structure difference between the image prompts and the pretrained NeRF models. To the best of our knowledge, this style transfer task is not achievable by existing single-image-to-3D methods. In Sample 2 for the textual prompt “An iron breastplate”, although both the textual and image prompt features are provided for 3D object synthesis, the generated result resembles a leather breastplate more closely, which aligns with the image prompt rather than the “iron” mentioned in the textual prompt. This illustrates that the image prompt exerts a stronger influence on the synthesis of the 3D object than the textual prompt. To further demonstrate the appearance guidance capability of IPSD in generating 3D objects, we use two samples whose reference image prompts are particularly complex and greatly different from the initial coarse NeRF models, as shown in Fig. 5. Even in such extreme cases, IPDreamer can still achieve high-quality 3D objects, such as the cyborg-style mini car generated in the first example, and the futuristic toy pistol in the second example. By utilizing IPDreamer’s style editing ability for 3D objects, the generated results can be more diverse.

## 4.2 Comparison with SOTA Text-to-3D Methods

In Fig. 6, we compare IPDreamer with four SOTA text-to-3D methods: DreamFusion [43], Magic3D [25], Fantasia3D [6], and ProlificDreamer [64]. With the





**Fig. 6:** Comparison with SOTA methods. Our results are not only high-quality but also controllable.

help of IPSD, IPDREAMER can generate highly controllable and realistic 3D objects that are consistent with the given image prompts. More samples are provided in the supplementary materials. We randomly select 20 textual prompts (see the supplementary material) and conduct a quantitative comparison in Table 1. Our IPDREAMER outperforms the SOTA methods. The lower FID score suggests the best quality of the 3D objects generated by IPDREAMER, while the higher CLIP score demonstrates that the generation results of IPDREAMER are more aligned with the provided textual prompts. How to calculate CLIP score and FID is detailed in the supplementary material.

### 4.3 User Study

To further verify the quality of our generated results, we follow previous works [6, 25, 64] and conduct a user study by comparing IPDREAMER with the four SOTA methods, under 16 randomly selected prompts (see the supplementary material). Each of 80 volunteers is provided with 16 pairs of results corresponding to the 16 prompts. In each pair, one from IPDREAMER and one from a randomly selected baseline. Thus, there are a total of 1280 pairwise comparisons. The volunteers are then asked to choose the better result in terms of faithfulness, quality, and fidelity. It is worth noting that the image prompts used in this study are generated based on the textual prompts, without any other guidance such as scribble images. The percentage of the preference in the user study is shown in Table 2, which indicates that our IPDREAMER outperforms all these text-to-3D methods.

### 4.4 Comparison with Zero-1-to-3 in Text-to-3D Generation

Existing single-image-to-3D generation methods are also capable of achieving text-to-3D generation. To demonstrate the effectiveness of IPSD, we present a comparison between IPDREAMER and Zero-1-to-3 in Fig. 7. We zoom in the



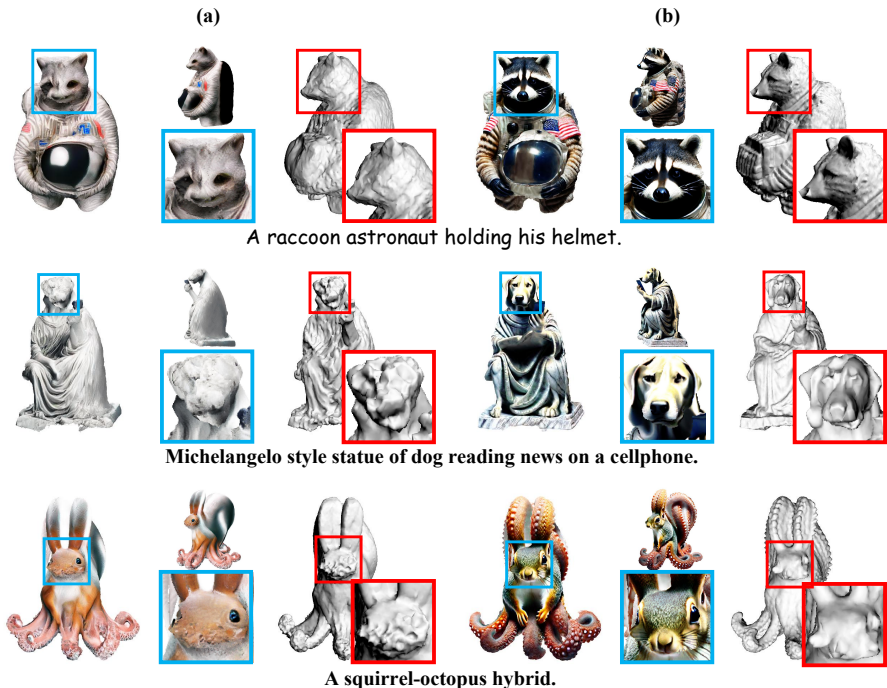


**Fig. 7:** Comparison with Zero-1-to-3 in text-to-3D generation. (a) 3D objects generated by Zero-1-to-3. (b) 3D objects generated by IPDreamer.

selected parts of the 3D objects and meshes to better compare the texture and geometry quality of the 3D objects produced by Zero-1-to-3 and our IPDreamer. Zero-1-to-3’s objects are quite blurry in many rendered images, and its meshes are very rough, indicating that current single-image-to-3D methods struggle with handling complex images. In contrast, the 3D objects generated by IPDreamer are of noticeably higher quality and more reasonable, with better geometric structures, thus proving the effectiveness of IPSD.

#### 4.5 Single Image to 3D

IPSD proposed in this paper can be integrated with other existing single-image-to-3D methods to enhance the quality of their generated results. Specifically, the quality of the 3D objects generated by these methods is relatively low in some viewpoints. However, the incorporation of IPSD can improve the quality of the rendered results in any viewpoint. In this work, we combine IPSD with Zero-1-to-3 to achieve single-image-to-3D generation (see the supplementary materials). As visualized in Fig. 8, compared with the 3D objects optimized by Zero-1-to-3 [28] and SyncDreamer [29], our IPDreamer can add more contextually appropriate

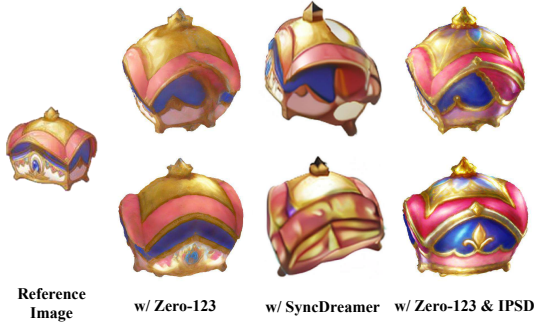


**Fig. 8:** 3D object optimization with different guidance methods based on the same image (left). The result guided by IPSD achieves the best quality.

**Table 3:** Ablation study of  $\delta_{geo}$

Methods	CLIP score $\uparrow$
w/o $\delta_{geo}$	0.8228
w/ $\delta_{geo}$	<b>0.8389</b>

details to the 3D object while preserving the identity of the reference image to achieve high-quality 3D object synthesis.

## 4.6 Ablation Study

We conduct an ablation study to evaluate the impact of  $\mathcal{L}_{IPSD-Geo}$  and  $\delta_{geo}$  on optimizing 3D objects. Their effectiveness is illustrated in Fig. 9 and Table 3. In Fig. 9, we showcase the optimized normal maps of two samples. After geometry optimization, Sample 1 and Sample 2 learn the high-frequency details from their corresponding image prompts. The difference in the optimized normal maps between Sample 1 and Sample 2 is readily discernible in Fig. 9, illustrating the efficacy of  $\mathcal{L}_{IPSD-Geo}$  in learning geometry representations from image prompts for style transfer. In Table 3, we compare the CLIP score of 3D objects optimized with and without  $\delta_{geo}$ . We conduct the quantitative comparison using the samples mentioned in Sec. 4.2 and employ CLIP score to compare the alignment of rendered images of 3D objects generated with and without  $\delta_{geo}$  in different viewpoints with the reference image prompt. The experimental results show that with  $\delta_{geo}$ , the rendered images of the 3D object in different viewpoints are more consistent with the reference image prompt.

## 5 Conclusion

In this work, we propose IPDreamer to achieve controllable high-quality 3D object generation. We introduce Image Prompt Score Distillation (IPSD) that employs image prompt adaption to provide detailed appearance information for better 3D object optimization. IPSD utilizes the reference image prompts and their corresponding normal maps to optimize the texture and geometry of 3D meshes, respectively. The experiments show that our IPDreamer is capable of generating appearance-controllable high-quality 3D objects. Improvements in 3D

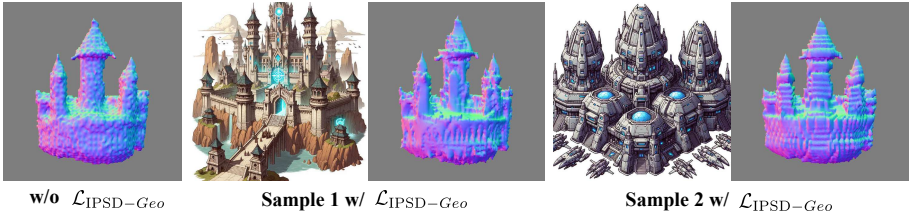


**Fig. 9:** Visualization of the initial normal map of the 3D object at the beginning of geometry optimization, along with the image prompt and the refined normal map after geometry optimization for each sample.

generation have often been constrained by the difficulty of obtaining 3D data, whereas optimizing the generation of rough 3D models and generating specific images are much simpler tasks. The significant breakthrough of this work lies in decomposing the 3D generation task into acquiring rough 3D models and optimizing 3D objects with the introduction of image prompt adaptation. Our IPDreamer not only elevates the quality of generated 3D objects, but also charts a new trajectory for future advancements and optimizations in 3D generation.

## References

- Brooks, T., Holynski, A., Efros, A.A.: Instructpix2pix: Learning to follow image editing instructions. In: CVPR (2023) [2](#), [4](#)
- Brown, T., Mann, B., Ryder, N., Subbiah, M., Kaplan, J.D., et al.: Language models are few-shot learners. In: NeurIPS (2020) [4](#)
- Chan, E.R., Lin, C.Z., Chan, M.A., Nagano, K., Pan, B., et al.: Efficient geometry-aware 3d generative adversarial networks. In: CVPR (2022) [4](#)
- Chan, E.R., Monteiro, M., Kellnhofer, P., Wu, J., Wetzstein, G.: pi-gan: Periodic implicit generative adversarial networks for 3d-aware image synthesis. In: CVPR (2021) [4](#)
- Chen, D.Z., Siddiqui, Y., Lee, H.Y., Tulyakov, S., Nießner, M.: Text2tex: Text-driven texture synthesis via diffusion models. arXiv preprint arXiv:2303.11396 (2023) [5](#)
- Chen, R., Chen, Y., Jiao, N., Jia, K.: Fantasia3d: Disentangling geometry and appearance for high-quality text-to-3d content creation. arXiv preprint arXiv:2303.13873 (2023) [1](#), [2](#), [5](#), [8](#), [11](#), [12](#), [20](#)
- Chen, Y., Zhang, C., Yang, X., Cai, Z., Yu, G., Yang, L., Lin, G.: It3d: Improved text-to-3d generation with explicit view synthesis. arXiv preprint arXiv:2308.11473 (2023) [5](#)
- Dhariwal, P., Nichol, A.: Diffusion models beat gans on image synthesis. In: NeurIPS (2021) [4](#)
- Gal, R., Patashnik, O., Maron, H., Bermano, A.H., Chechik, G., Cohen-Or, D.: Stylegan-nada: Clip-guided domain adaptation of image generators. ToG (2022) [20](#)
- Gao, S., Liu, X., Zeng, B., Xu, S., Li, Y., Luo, X., Liu, J., Zhen, X., Zhang, B.: Implicit diffusion models for continuous super-resolution. arXiv preprint arXiv:2303.16491 (2023) [4](#)

11. Gu, J., Liu, L., Wang, P., Theobalt, C.: Stylenerf: A style-based 3d-aware generator for high-resolution image synthesis. arXiv preprint arXiv:2110.08985 (2021) 4
12. Hao, Z., Mallya, A., Belongie, S., Liu, M.Y.: Gancraft: Unsupervised 3d neural rendering of minecraft worlds. In: CVPR (2021) 4
13. Haque, A., Tancik, M., Efros, A.A., Holynski, A., Kanazawa, A.: Instruct-nerf2nerf: Editing 3d scenes with instructions. arXiv preprint arXiv:2303.12789 (2023) 4
14. Heusel, M., Ramsauer, H., Unterthiner, T., Nessler, B., Hochreiter, S.: Gans trained by a two time-scale update rule converge to a local nash equilibrium (2017) 22
15. Ho, J., Chan, W., Saharia, C., Whang, J., Gao, R., et al.: Imagen video: High definition video generation with diffusion models. arXiv:2210.02303 (2022) 4
16. Ho, J., Jain, A., Abbeel, P.: Denoising diffusion probabilistic models. In: NeurIPS (2020) 4
17. Ho, J., Salimans, T., Gritsenko, A., Chan, W., Norouzi, M., Fleet, D.J.: Video diffusion models. In: NeurIPS (2022) 4
18. Hu, E.J., Shen, Y., Wallis, P., Allen-Zhu, Z., Li, Y., Wang, S., Wang, L., Chen, W.: Lora: Low-rank adaptation of large language models. arXiv preprint arXiv:2106.09685 (2021) 2, 4, 6
19. Huang, L., Chen, D., Liu, Y., Shen, Y., Zhao, D., Zhou, J.: Composer: Creative and controllable image synthesis with composable conditions. arXiv preprint arXiv:2302.09778 (2023) 4
20. Jain, A., Mildenhall, B., Barron, J.T., Abbeel, P., Poole, B.: Zero-shot text-guided object generation with dream fields. In: CVPR (2022) 1, 2, 4
21. Kong, Z., Ping, W., Huang, J., Zhao, K., Catanzaro, B.: Diffwave: A versatile diffusion model for audio synthesis. arXiv:2009.09761 (2020) 4
22. Kulikov, V., Yadin, S., Kleiner, M., Michaeli, T.: Sinddm: A single image denoising diffusion model. In: PMLR (2022) 4
23. Li, H., Yang, Y., Chang, M., Chen, S., Feng, H., Xu, Z., Li, Q., Chen, Y.: Srdiff: Single image super-resolution with diffusion probabilistic models. Neurocomputing (2022) 4
24. Li, M., Duan, Y., Zhou, J., Lu, J.: Diffusion-sdf: Text-to-shape via voxelized diffusion. arXiv:2212.03293 (2022) 4
25. Lin, C.H., Gao, J., Tang, L., Takikawa, T., Zeng, X., Huang, X., Kreis, K., Fidler, S., Liu, M.Y., Lin, T.Y.: Magic3d: High-resolution text-to-3d content creation. In: CVPR (2023) 1, 2, 5, 11, 12, 20
26. Liu, J., Li, C., Ren, Y., Chen, F., Liu, P., Zhao, Z.: Diffsinger: Diffusion acoustic model for singing voice synthesis. arXiv:2105.02446 (2021) 4
27. Liu, M., Xu, C., Jin, H., Chen, L., Xu, Z., Su, H.: One-2-3-4-5: Any single image to 3d mesh in 45 seconds without per-shape optimization. arXiv preprint arXiv:2306.16928 (2023) 5
28. Liu, R., Wu, R., Van Hoorick, B., Tokmakov, P., Zakharov, S., Vondrick, C.: Zero-1-to-3: Zero-shot one image to 3d object. arXiv preprint arXiv:2303.11328 (2023) 2, 3, 5, 6, 13
29. Liu, Y., Lin, C., Zeng, Z., Long, X., Liu, L., Komura, T., Wang, W.: Syncdreamer: Generating multiview-consistent images from a single-view image. arXiv preprint arXiv:2309.03453 (2023) 2, 5, 13
30. Lugmayr, A., Danelljan, M., Romero, A., Yu, F., Timofte, R., Van Gool, L.: Repaint: Inpainting using denoising diffusion probabilistic models. In: CVPR (2022) 4
31. Luo, S., Hu, W.: Diffusion probabilistic models for 3d point cloud generation. In: CVPR (2021) 4

32. Melas-Kyriazi, L., Laina, I., Rupperecht, C., Vedaldi, A.: Realfusion: 360deg reconstruction of any object from a single image. In: CVPR (2023) 5
33. Mildenhall, B., Srinivasan, P.P., Tancik, M., Barron, J.T., Ramamoorthi, R., Ng, R.: Nerf: Representing scenes as neural radiance fields for view synthesis. COMMUN ACM (2021) 1, 3, 4
34. Mohammad Khalid, N., Xie, T., Belilovsky, E., Popa, T.: Clip-mesh: Generating textured meshes from text using pretrained image-text models. In: SIGGRAPH Asia (2022) 1, 2, 4
35. Mokady, R., Hertz, A., Aberman, K., Pritch, Y., Cohen-Or, D.: Null-text inversion for editing real images using guided diffusion models. In: CVPR (2023) 4
36. Mou, C., Wang, X., Xie, L., Zhang, J., Qi, Z., Shan, Y., Qie, X.: T2i-adapter: Learning adapters to dig out more controllable ability for text-to-image diffusion models. arXiv preprint arXiv:2302.08453 (2023) 4
37. Müller, T., Evans, A., Schied, C., Keller, A.: Instant neural graphics primitives with a multiresolution hash encoding. ToG (2022) 1
38. Munkberg, J., Hasselgren, J., Shen, T., Gao, J., Chen, W., Evans, A., Müller, T., Fidler, S.: Extracting triangular 3d models, materials, and lighting from images. In: CVPR (2022) 8
39. Nguyen-Phuoc, T., Li, C., Theis, L., Richardt, C., Yang, Y.L.: Hologan: Unsupervised learning of 3d representations from natural images. In: ICCV (2019) 4
40. Nichol, A., Dhariwal, P., Ramesh, A., Shyam, P., Mishkin, P., McGrew, B., Sutskever, I., Chen, M.: Glide: Towards photorealistic image generation and editing with text-guided diffusion models. arXiv preprint arXiv:2112.10741 (2021) 2, 4
41. Niemeyer, M., Geiger, A.: Giraffe: Representing scenes as compositional generative neural feature fields. In: CVPR (2021) 4
42. Peebles, W., Xie, S.: Scalable diffusion models with transformers. arXiv:2212.09748 (2022) 4
43. Poole, B., Jain, A., Barron, J.T., Mildenhall, B.: Dreamfusion: Text-to-3d using 2d diffusion. arXiv preprint arXiv:2209.14988 (2022) 1, 2, 5, 9, 11, 20
44. Qi, Z., Zhang, X., Cheng, N., Xiao, J., Wang, J.: Diftalker: Co-driven audio-image diffusion for talking faces via intermediate landmarks. arXiv preprint arXiv:2309.07509 (2023) 4
45. Qian, G., Mai, J., Hamdi, A., Ren, J., Siarohin, A., Li, B., Lee, H.Y., Sko-rokhodov, I., Wonka, P., Tulyakov, S., Bernard, G.: Magic123: One image to high-quality 3d object generation using both 2d and 3d diffusion priors. arXiv preprint arXiv:2306.17843 (2023) 5
46. Radford, A., Kim, J.W., Hallacy, C., Ramesh, A., Goh, G., et al.: Learning transferable visual models from natural language supervision. In: ICML (2021) 4
47. Ranftl, R., Bochkovskiy, A., Koltun, V.: Vision transformers for dense prediction. In: ICCV (2021) 6
48. Rombach, R., Blattmann, A., Lorenz, D., Esser, P., Ommer, B.: High-resolution image synthesis with latent diffusion models. In: CVPR (2022) 1, 2, 4, 8
49. Saharia, C., Chan, W., Saxena, S., Li, L., Whang, J., Jonathan, H., et al.: Photorealistic text-to-image diffusion models with deep language understanding. In: NeurIPS (2022) 1, 4
50. Saharia, C., Ho, J., Chan, W., Salimans, T., Fleet, D.J., Norouzi, M.: Image super-resolution via iterative refinement. TPAMI (2022) 4
51. Shen, T., Gao, J., Yin, K., Liu, M.Y., Fidler, S.: Deep marching tetrahedra: a hybrid representation for high-resolution 3d shape synthesis. In: NeurIPS (2021) 6, 7, 8

52. Shi, Y., Wang, P., Ye, J., Long, M., Li, K., Yang, X.: Mvdream: Multi-view diffusion for 3d generation. arXiv preprint arXiv:2308.16512 (2023) [2](#), [5](#)
53. Sohl-Dickstein, J., Weiss, E., Maheswaranathan, N., Ganguli, S.: Deep unsupervised learning using nonequilibrium thermodynamics. In: ICML (2015) [4](#)
54. Song, J., Meng, C., Ermon, S.: Denoising diffusion implicit models. arXiv:2010.02502 (2020) [4](#)
55. Takagi, Y., Nishimoto, S.: High-resolution image reconstruction with latent diffusion models from human brain activity. biorxiv. In: CVPR (2022) [4](#)
56. Takagi, Y., Nishimoto, S.: High-resolution image reconstruction with latent diffusion models from human brain activity. In: CVPR (2023) [4](#)
57. Tang, J., Wang, T., Zhang, B., Zhang, T., Yi, R., Ma, L., Chen, D.: Make-it-3d: High-fidelity 3d creation from a single image with diffusion prior. arXiv preprint arXiv:2303.14184 (2023) [5](#)
58. Tevet, G., Raab, S., Gordon, B., Shafir, Y., Cohen-Or, D., Bermano, A.H.: Human motion diffusion model. arXiv:2209.14916 (2022) [4](#)
59. Touvron, H., Lavril, T., Izacard, G., Martinet, X., Lachaux, M.A., et al.: Llama: Open and efficient foundation language models. arXiv preprint arXiv:2302.13971 (2023) [4](#)
60. Touvron, H., Martin, L., Stone, K., Albert, P., Almahairi, A., et al.: Llama 2: Open foundation and fine-tuned chat models. arXiv preprint arXiv:2307.09288 (2023) [4](#)
61. Vahdat, A., Kreis, K., Kautz, J.: Score-based generative modeling in latent space. In: NeurIPS (2021) [4](#)
62. Wang, Q., Bai, X., Wang, H., Qin, Z., Chen, A.: Instantid: Zero-shot identity-preserving generation in seconds. arXiv preprint arXiv:2401.07519 (2024) [3](#)
63. Wang, W., Bao, J., Zhou, W., Chen, D., Chen, D., Yuan, L., Li, H.: Sindiffusion: Learning a diffusion model from a single natural image. arXiv:2211.12445 (2022) [4](#)
64. Wang, Z., Lu, C., Wang, Y., Bao, F., Li, C., Su, H., Zhu, J.: Prolificdreamer: High-fidelity and diverse text-to-3d generation with variational score distillation. arXiv preprint arXiv:2305.16213 (2023) [1](#), [2](#), [5](#), [8](#), [11](#), [12](#), [20](#), [25](#)
65. Xie, X., Zhou, P., Li, H., Lin, Z., Yan, S.: Adan: Adaptive nesterov momentum algorithm for faster optimizing deep models. arXiv preprint arXiv:2208.06677 (2022) [20](#)
66. Yang, J., Cheng, Z., Duan, Y., Ji, P., Li, H.: Consistnet: Enforcing 3d consistency for multi-view images diffusion. arXiv preprint arXiv:2310.10343 (2023) [5](#)
67. Ye, H., Zhang, J., Liu, S., Han, X., Yang, W.: Ip-adapter: Text compatible image prompt adapter for text-to-image diffusion models. arXiv preprint arXiv:2308.06721 (2023) [3](#), [4](#), [6](#)
68. Zhang, K., Mo, L., Chen, W., Sun, H., Su, Y.: Magicbrush: A manually annotated dataset for instruction-guided image editing. arXiv preprint arXiv:2306.10012 (2023) [4](#)
69. Zhang, L., Agrawala, M.: Adding conditional control to text-to-image diffusion models. arXiv preprint arXiv:2302.05543 (2023) [2](#), [4](#), [7](#)
70. Zhang, Y., Liu, J., Song, Y., Wang, R., Tang, H., Yu, J., Li, H., Tang, X., Hu, Y., Pan, H., et al.: Ssr-encoder: Encoding selective subject representation for subject-driven generation. arXiv preprint arXiv:2312.16272 (2023) [3](#)
71. Zhao, M., Zhao, C., Liang, X., Li, L., Zhao, Z., Hu, Z., Fan, C., Yu, X.: Efficientdreamer: High-fidelity and robust 3d creation via orthogonal-view diffusion prior. arXiv preprint arXiv:2308.13223 (2023) [5](#)

72. Zhao, S., Chen, D., Chen, Y.C., Bao, J., Hao, S., Yuan, L., Wong, K.Y.K.: Uni-controlnet: All-in-one control to text-to-image diffusion models. arXiv preprint arXiv:2305.16322 (2023) [4](#)

# Appendix

In this supplementary, we first provide more generated 3D objects of texture editing and text-to-3D in Section A and Section B. Then we elaborate training details of IPDREAMER in Section C. Finally, we discuss the limitation and social impact of IPDREAMER in Section D and Section E.

## A More Examples of Texture Editing

To further demonstrate IPDREAMER’s remarkable ability to manipulate appearance, we conduct more texture editing experiments. These experiments use diverse textual prompts, each accompanied by two distinct image prompts. As evident in Fig. A, IPDREAMER consistently produces impressive 3D object synthesis, regardless of the geometric shape of the NeRF acquired in Stage 1 or the image prompts used for texture editing. The generated results highlight IPDREAMER’s powerful texture editing capabilities for 3D objects, suggesting its potential to serve effectively in the 3D gaming and video industries.

## B Comparison of Text-to-3D

The textual prompts we used in Section 4.2 of the main paper are shown in Table A. And we provide more comparison results between IPDREAMER and other four SOTA methods [6, 25, 43, 64] in Fig. B.

## C Training Detail

### C.1 Implementaion Details

*Optimization.* In this work, we conduct all of our experiments on one A100-SXM4-40GB GPU. In Stage 1, we optimize  $5k$  steps with Adam optimizer [65] to obtain a NeRF model. In Stage 2, we optimize  $10k$  steps for geometry optimization and  $15k$  steps for texture optimization. During each optimization progress in Stage 2, we initially sample the timesteps  $t \sim \mathcal{U}(0.02, 0.98)$  for the first  $5k$  steps, and then sample  $t$  from  $t \sim \mathcal{U}(0.02, 0.5)$  for the rest steps. Each optimization process in Stage 2 requires approximately 9GB GPU memory with batch size 1 and a rendering resolution of 512.

*Metrics.* We perform quantitative comparisons to evaluate IPDREAMER’s performance, with the following metrics:

- CLIP score [9]: We employ CLIP score in Section 4.2 of the main paper. By assessing the alignment between the textual descriptions and the rendered images of 3D objects from various viewpoints, we can judge whether text-to-3D methods successfully generate 3D objects that match the input textual prompts.



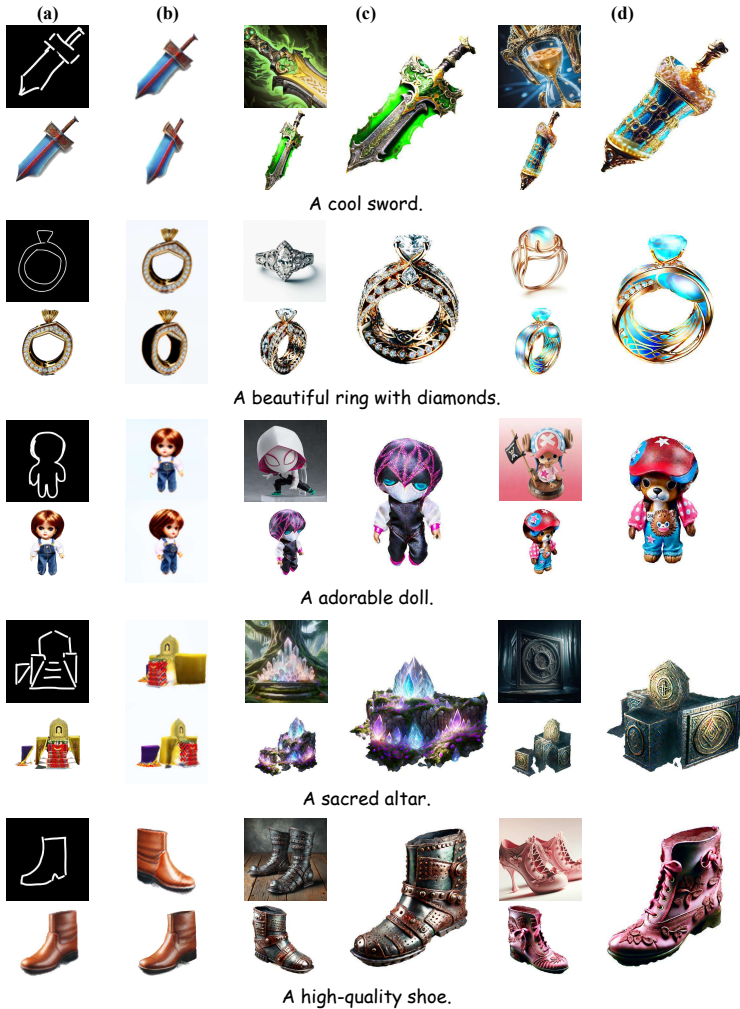


**Fig. A:** Edited 3D objects with different image prompts. (a) Scribble object outlines and corresponding image prompts generated by ControlNet. (b) Rendering of NeRFs from Stage 1. (c) (d) Two samples demonstrated for each textual prompt. In each sample, the top left is a selected image prompt, and the bottom left and the right illustrate the 3D object optimized by IPDreamer based on the NeRF from Stage 1.

---

A praying mantis wearing roller.
Michelangelo-style statue of a dog reading news on a cellphone.
A matte painting of a castle made of cheesecake surrounded by a moat made of ice cream.
A chimpanzee dressed like Henry VIII king of England.
A 3D model of an adorable cottage with a thatched roof.
A plate piled high with chocolate chip cookies.
A vintage record player.
A car made out of cheese.
A beautifully carved wooden knight chess piece.
A car made out of sushi.
A squirrel-octopus hybrid.
A small saguaro cactus is planted in a clay pot.
A DSLR photo of an imperial state crown of England.
A rotary telephone carved out of wood.
A raccoon astronaut holding his helmet.
A classic Packard car.
A cauldron full of gold coins.
A blue tulip.
A stuffed grey rabbit holding a pretend carrot.
A plush dragon toy.

---

**Table A:** Textual prompts used in the user study.

- Fréchet Inception Distance (FID) [14]: To evaluate the quality of the generated results, we utilize FID to compare the similarity between the rendering images of 3D objects and the images generated by the text-to-image model, Stable Diffusion.

## C.2 Cross Attention for Image Prompts

In this section, we describe how IPDreamer employs the image prompt in Stable Diffusion to guide the mesh optimization with a textual prompt. Given the query features  $Z$ , textual prompt embedding  $c_t$ , and image prompt embedding  $y_{rgb}$ , IPSD employs two cross-attention layers for  $c_t$  and  $y_{rgb}$ , respectively. The cross attention  $Z'$  is computed as:

$$Z' = \text{Softmax}\left(\frac{QK^\top}{\sqrt{d}}\right)V + \text{Softmax}\left(\frac{Q(K')^\top}{\sqrt{d}}\right)V', \quad (\text{A.1})$$

where  $Q = ZW_q$ ,  $K = c_tW_k$ ,  $V = c_tW_v$ ,  $K' = y_{rgb}W'_k$ ,  $V' = y_{rgb}W'_v$  are the corresponding query, keys, and values of the cross-attention modules, respectively, and  $W_q$ ,  $W_k$ ,  $W_v$ ,  $W'_k$ ,  $W'_v$  are the linear projection matrices.

## C.3 Details of Single-Image to 3D

As mentioned in the main paper, our IPDreamer can perform single-image-to-3D generation. In this section, we describe how we combine  $\mathcal{L}_{\text{IPSD-}Tex}$  and

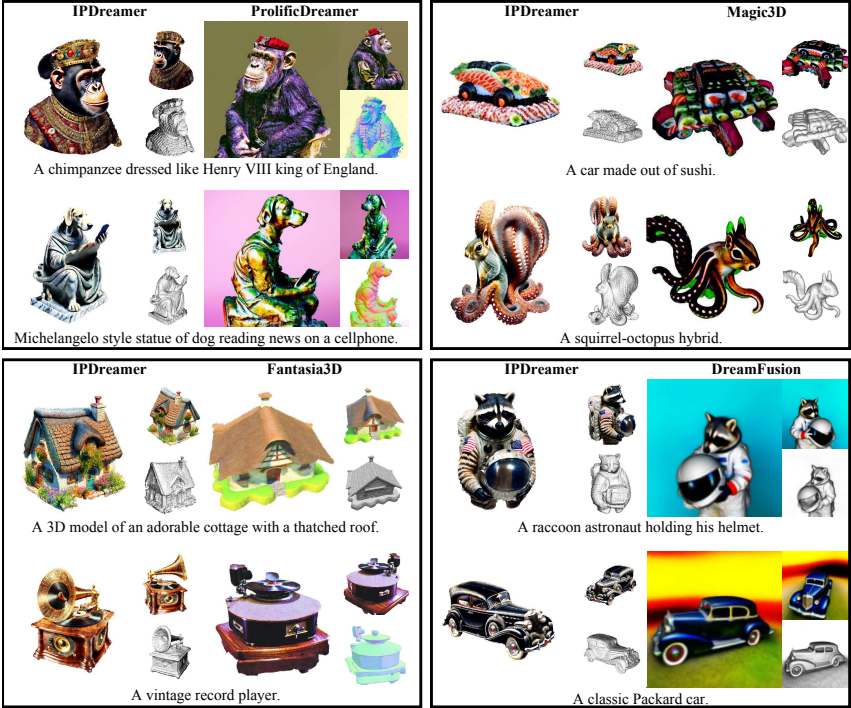


**Fig. B:** Eight examples of text-to-3D.

$\mathcal{L}_{\text{Zero123-SDS}}$  in texture optimization. Using  $\mathcal{L}_{\text{Zero123-SDS}}$  alone to supervise the single-image-to-3D generation may lead to the results that the generated 3D objects are inconsistent when viewed from different directions, as demonstrated in Fig. C. Therefore, we leverage both  $\mathcal{L}_{\text{IPSD-}Tex}$  and  $\mathcal{L}_{\text{Zero123-SDS}}$  to supervise the 3D generation simultaneously. The supervision gradients of the combined loss  $\mathcal{L}_{\text{IPSD-}Tex\text{-}Zero123}$  are defined as follows:

$$\begin{aligned}
 & \nabla_{\theta} \mathcal{L}_{\text{IPSD-}Tex\text{-}Zero123}(\theta, \Delta V, S) = \\
 & \mathbb{E}_{t_1, t_2, \epsilon_1, \epsilon_2} [(\alpha_1(w(t_1) \epsilon_{ip}(z_{rgb, t_1}; y_{rgb} + \delta_{geo}, y, t_1) - \epsilon_1) \\
 & + \alpha_2(w(t_2) \epsilon_{zero123}(z_{rgb, t_2}; I_{rgb}, R, T, t_2) - \epsilon_2)) \frac{\partial z_{rgb}}{\partial \theta}], \tag{A.2}
 \end{aligned}$$

$$\begin{aligned}
 & \nabla_{\Delta V} \mathcal{L}_{\text{IPSD-}Tex\text{-}Zero123}(\theta, \Delta V, S) = \\
 & \mathbb{E}_{t_1, t_2, \epsilon_1, \epsilon_2} [(\alpha_1(w(t_1) \epsilon_{ip}(z_{rgb, t_1}; y_{rgb} + \delta_{geo}, y, t_1) - \epsilon_1) \\
 & + \alpha_2(w(t_2) \epsilon_{zero123}(z_{rgb, t_2}; I_{rgb}, R, T, t_2) - \epsilon_2)) \frac{\partial z_{rgb}}{\partial \Delta V}], \tag{A.3}
 \end{aligned}$$



**Fig. C:** Comparison of single-image-to-3D. The result with both  $\mathcal{L}_{\text{Zero123-SDS}}$  and  $\mathcal{L}_{\text{IPSD-TeX}}$  reduces unnatural artifacts, leading to a more accurate and realistic 3D model.

$$\begin{aligned} \nabla_S \mathcal{L}_{\text{IPSD-TeX-Zero123}}(\theta, \Delta V, S) = & \\ \mathbb{E}_{t_1, t_2, \epsilon_1, \epsilon_2} [ & (\alpha_1 (w(t_1) \epsilon_{ip}(z_{rgb, t_1}; y_{rgb} + \delta_{geo}, y, t_1) - \epsilon_1) \\ & + \alpha_2 (w(t_2) \epsilon_{zero123}(z_{rgb, t_2}; I_{rgb}, R, T, t_2) - \epsilon_2)) \frac{\partial z_{rgb}}{\partial S} ], \end{aligned} \quad (\text{A.4})$$

where  $\theta$ ,  $\delta_{geo}$ ,  $\Delta V$ ,  $S$ ,  $R$ , and  $T$  are the corresponding parameters mentioned in the main paper, and  $\alpha_1$  and  $\alpha_2$  are the balancing parameters. Eq. A.2, Eq. A.3, and Eq. A.4 are modified based on Eq. 8, Eq. 9, and Eq. 10 in the main paper, respectively.



**Fig. D:** Limitations. Our IPDreamer can effectively edit 3D objects and generate high-quality 3D models according to image prompts. However, as shown in (c), when a provided image prompt is quite different from the generated 3D object in (b), the edited 3D model is more like “a high-quality painting” rather than “an adorable doll”.

## D Limitation and Discussion

IPDreamer demonstrates its capability in synthesizing high-quality 3D models and notably in editing the style of these models guided by provided image prompts. However, it is time-intensive in optimization, requiring several hours

for each model. Although it is faster than ProlificDreamer [64], it is still much slower compared to image generation used by Generative Adversarial Networks (GANs) or Diffusion Models. Additionally, while our method facilitates texture editing impressively, it does not offer complete control over the style transfer from additional image prompts to the 3D object, as depicted in Fig. D. Addressing these limitations will be the focus of our future research.

## E Social Impact

Our IPDreamer does not have a direct negative impact on society. However, it's important to recognize the potential of high-quality 3D objects and ensure they are not adopted for malicious purposes.